Journal of the Korean Astronomical Society
47: 105 ∼ 113, 2014 June

http://dx.doi.org/10.5303/JKAS.2014.47.3.105
pISSN: 1225-4614 · eISSN: 2288-890X
http://jkas.kas.org

Asymmetry of Magnetic Helicity Flux in Emerging Bipolar Active Regions

Dan Yang[1,2], Yunchun Jiang[1], Jiayan Yang[1], Yi Bi[1], and Bo Yang[1,2]

[1]Yunnan Observatories, Chinese Academy of Sciences, P.O. Box 110, Kunming 650011, China; yangdan@ynao.ac.cn
[2]University of Chinese Academy of Sciences, Beijing 100049, China

Received April 9, 2014; accepted May 10, 2014

Abstract: We apply differential affine velocity estimator (DAVE) to the Solar Dynamics Observatory (SDO)/Helioseismic and Magnetic Imager (HMI) 12-min line-of-sight magnetograms, and separately calculate the injected magnetic helicity for the leading and the following polarities of nine emerging bipolar active regions (ARs). Comparing magnetic helicity flux of the leading polarity with the following polarity, we find that six ARs studied in this paper have the following polarity that injected more magnetic helicity flux than that of the leading polarity. We also measure the mean area of each polarity in all the nine ARs, and find that the compact polarity tend to possess more magnetic helicity flux than the fragmented one. Our results confirm the previous studies on asymmetry of magnetic helicity that emerging bipolar ARs have a polarity preference in injecting magnetic helicity. Based on the changes of unsigned magnetic flux, we divide the emergence process into two evolutionary stages: (1) an increasing stage before the peak flux and (2) a constant or decreasing stage after the peak flux. Obvious changes on magnetic helicity flux can be seen during transition from one stage to another. Seven ARs have one or both polarity that changed the sign of magnetic helicity flux. Additionally, the prevailing polarity of the two ARs, which injects more magnetic helicity, changes form the following polarity to the leading one.

Key words: Sun: interior — Sun: magnetic fields — Sun: photosphere

1. Introduction

Magnetic helicity, which is defined as $\int \mathbf{A}\cdot\mathbf{B}d^3x$, where $\mathbf{B}$ is the magnetic field and $\mathbf{A}$ is the vector potential, measures the twist, kink, and the inter-linkage of magnetic field lines. Theoretical studies on magnetic helicity show that magnetic helicity is conserved in ideal plasma and dissipates very slowly in the course of magnetic reconnection when the local plasma possesses a high magnetic Reynolds number (Woltjer 1958; Berger & Field 1984). When the magnetic helicity is conserved, the magnetic field will relax into a minimum-energy state, which is a force-free field with a constant α and all the magnetic fields share the same amount of total magnetic helicity (Woltjer 1958). Applying the conservation of magnetic helicity as confinement in the energy release process, Taylor relaxation successfully predicted the observed field reversals in the laboratory pinch devices (Taylor 1974, 1986). This was a huge triumph to employ magnetic helicity to explain the behavior of plasma with the energy release process. Since then, many attempts have been made to apply the Taylor relaxation to the solar atmosphere. Observations indicate that magnetic helicity can be injected into the corona by flux emergence (Leka et al. 1996). In each hemisphere, helicity has a preferred sign in injecting, namely, positive/negative sign in the southern/northern hemisphere (Rust 1994; Pevtsov et al. 1995; Pevtsov & Balasubramaniam 2003; Démoulin & Pariat 2009; Yeates & Mackay 2009; Wang & Zhang 2010; Zhang et al. 2010; Hao & Zhang 2011; Pipin et al. 2013; Wang 2013). This hemisphere helicity rule could set restriction on the dynamo theory, since the observed helicity should originated from the dynamo process. Considering that the magnetic helicity cannot dissipate in the corona, the injected helicity will be accumulated in the corona, and thus may play a key role in various solar phenomena such as flares, filament/prominence eruptions, and coronal mass ejections (CMEs) (Berger M. A. 1984; Rust 1994; Low 1996; Wang et al. 2004; Leka et al. 2005; Zhang et al. 2006; Pevtsov 2008; Zhang et al. 2008; Démoulin & Pariat 2009). However, the origin of the observed magnetic helicity in the solar atmosphere is not yet well understood.

Currently, there are two prevailing scenarios explaining the formation of the observed magnetic helicity in the active regions (ARs). One is the α-effect of mean-field magnetohydrodynamics (MHD), where generates a mean electromotive force along the mean magnetic field by turbulently fluctuating parts of the velocity and the magnetic field, could subsequently generate small-scale and large-scale magnetic helicities of opposite sign simultaneously (Seehafer 1996). The other is the so-called Σ-effect, which operates on isolated magnetic flux tubes subjected to buffeting by turbulence with a non-vanishing kinetic helicity, that could produce twist of one sign and the same amount of writhe with the opposite sign (Longcope et al. 1998; Longcope & Pevtsov 2003). Both the theories are based on the MHD theory and requires information of the convection zone (CZ), which, theoretically, can be obtained by helioseismic in-

Corresponding author: D. Yang

versions of solar oscillation measurements (Schou et al. 1998). The sign of the twist predicted by the Σ-effect is opposite to that of the α-effect, but it agrees with the observation (Longcope et al. 1998). Due to lack of a proper method, we can not probe the α-effect or the Σ-effect directly. For the Σ-effect, some sophisticated knowledge such as the kinetic helicity of the CZ is, at present, restricted only to the shallow layer of the solar subsurface (Zhao & Kosovichev 2004). Moreover, there is no detailed theoretical predictions that concern the α-effect in the solar convection zone. All these facts urge us to perform more studies to answer the origin of the magnetic helicity.

A recent study on the asymmetry of magnetic helicity sheds light on solving the origin of magnetic helicity in the ARs. By using local correlation tracking (LCT) to the Michelson Doppler Image (MDI) 96-min line-of-sight magnetograms for 15 emerging bipolar ARs, Tian & Alexander (2009) showed a spatial discrepancy in the total magnetic helicity flux of these ARs, they found that the leading polarity injected typically 3 to 10 times more magnetic helicity than the following polarity. Further studies confirmed this result for 3 emerging bipolar ARs, by applying differential affine velocity estimator (DAVE) to the MDI 1-min high spatial resolution line-of-sight magnetograms (Tian et al. 2011). Since the observed magnetic helicity carried by the emerging flux should originate from the CZ, such asymmetry gives us more knowledge to figure out what happened to the magnetic flux tubes when they were rising through the CZ. Moreover, it may also help to set more confinements on the dynamo process, such as the initial twist of the magnetic flux tubes before they rise through the CZ. However, certain issues need to be sorted before such asymmetry is applied to the dynamo theory. Firstly, the results we have were yielded from the MDI data only, and the previous study focused only on the emerging bipolar ARs that have a compact leading polarity and a fragmented following one. Secondly, detailed evolutionary information of this asymmetry remains a mystery: i.e., we do not know wether this asymmetry vary with time or not. Therefore, further studies need to be carried out on the asymmetry of magnetic helicity and its temporal variations using the data observed by some advanced instruments.

The purpose of this paper is to perform further study on the asymmetry of magnetic helicity between two polarities of emerging bipolar ARs. We calculated the injected magnetic helicity of 9 emerging bipolar ARs dating from May to December 2010, by applying DAVE to the Solar Dynamics Observatory (SDO)/Helioseismic and Magnetic Imager (HMI) 12-min line-of-sight high resolution magnetograms. Comparing the magnetic helicity flux of the leading polarity with the following polarity, we found that 6 out of the 9 ARs have the following polarity that injected more magnetic helicity flux than that of the leading polarity. To see whether the discrepancy of magnetic helicity between the polarities evolves with time, we divided the emergence process into two evolutionary stages, based on the changes of unsigned magnetic flux. A clear difference in the magnetic helicity flux between the two evolutionary stages was found.

2. Method and Observations

Huge progress in measuring the magnetic helicity in the Sun has been achieved in the past two decades. Wang (1996) first estimated the magnetic helicity injection rate through the photosphere. Later, Chae (2001) measured the magnetic helicity injected through photosphere by employing local correlation tracking (LCT) to MDI line-of-sight magnetograms to track the photospheric flows. However, the LCT method did not agree with the magnetic induction equation. Therefore, a method called differential affine velocity estimator (DAVE) was used to solve this problem (Schuck 2005, 2006). DAVE uses affine velocity files, to describe a velocity field inside a local area around a point (x_i, y_i) with six parameters: U_i, $U_{x,i}$, $U_{y,i}$, V_i, $V_{x,i}$, $V_{y,i}$. The velocity $\mathbf{u}$ satisfies the magnetic induction equation for each local window. Compared to LCT, DAVE method is better in measuring magnetic helicity (Schuck 2006; Chae 2007).

To monitor the spatial distribution of the injected magnetic helicity, magnetic helicity flux density is a good proxy (Chae 2001; Liu & Zhang 2006; Démoulin & Pariat 2009). The density can be written as

$$G_A(\mathbf{x}) = -2(\mathbf{A}_p \cdot \mathbf{u})B_n, \tag{1}$$

where, $\mathbf{A}_p$ is the vector potential defined by Berger & Field (1984). Unfortunately, calculating magnetic helicity flux with this density may yield fake polarities. Pariat et al. (2005, 2006) proposed a new way to calculate magnetic helicity flux density, which satisfies,

$$G_\theta(\mathbf{x}) = -\frac{B_n(\mathbf{x})}{2\pi}\int_{S'}\frac{((\mathbf{x}-\mathbf{x}')\times(\mathbf{u}-\mathbf{u}'))|_n}{|\mathbf{x}-\mathbf{x}'|^2}B_n(\mathbf{x}')dS', \tag{2}$$

where $\mathbf{x}$ and $\mathbf{x}'$ are the photospheric magnetic foot points and the subscript n denotes the normal component of a vector. It is well accepted that this method is significantly effective in reducing fake polarities.

In this paper, we apply DAVE to calculate the velocity of photosphere flow with line-of-sight magnetograms and adopt G_θ to calculate the magnetic helicity density. The magnetograms are from SDO/HMI, which provides full-disk magnetograms observed in the Fe I 6173$\mathring{A}$ absorption line, with a spatial sampling of $0.5''$ pixel^{-1}, and a noise level of approximately 10 G (Wachter et al. 2012). It has been found that the measurement of the DAVE method works well at a time interval $\Delta t = 10$ minutes (Tian et al. 2011). Considering HMI provides 45-s cadence and 12-min cadence (lower noise) line-of-sight magnetograms, we chose a time interval of 12 minutes, which is close to 10 minutes, and used 12-min longitude magnetograms in this work. As for the window size, we chose 15×15 pixels, taking into account the shapes of the ARs we studied (Welsch et al. 2007; Schuck 2008; Tian et al. 2011).

We measured the injected magnetic helicity of 9 bipolar emerging ARs. All ARs emerged near the disk center and processed well-formed bipolar structure during the observation. The ARs were found by the HMI Active Region Patches (HARPs) program, which automatically identified all magnetic regions above a certain flux. Five of the ARs, having an NOAA number, are AR 11072, 11076, 11120, 11124, and 11130. The other four ARs, are too small to have NOAA numbers, but are identified the by HARP program. These ARs are HARP 0044, 0047, 0228, and 0296. Following Tian & Alexander (2009), we considered the region of magnetic flux greater than 20G (less than -20G) as positive (negative) polarity. In our work, we did not consider the contribution of differential rotation in injecting magnetic helicity, as its contribution is negligible in emerging ARs. Thus, all the magnetograms were differentially rotated with respect to the disc center (Démoulin et al. 2002; Démoulin & Pariat 2009).

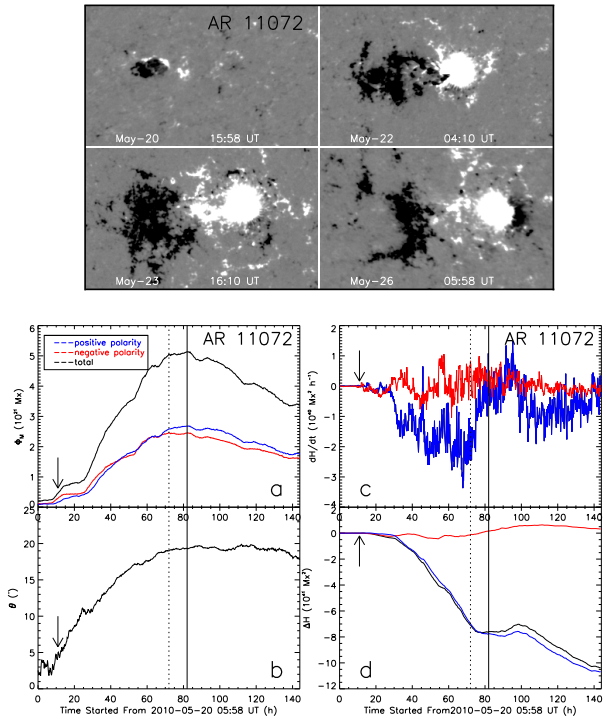

Figure 1. The top panels are snapshots of the four HMI 12-min line-of-sight magnetograms of AR 11072. The bottom panels are the changes of the magnetic flux (a), polarity distance (b), magnetic helicity injection rate (c), and the accumulated magnetic helicity flux (d) in AR 11072. The blue and red curves denote the flux of positive and negative polarity, respectively. The arrows mark the first emergence, and the vertical solid lines indicate the time when the unsigned magnetic flux reached its maximum, and the vertical dotted lines mark the time when AR 11072 passed through the central meridian on the observed solar disk.

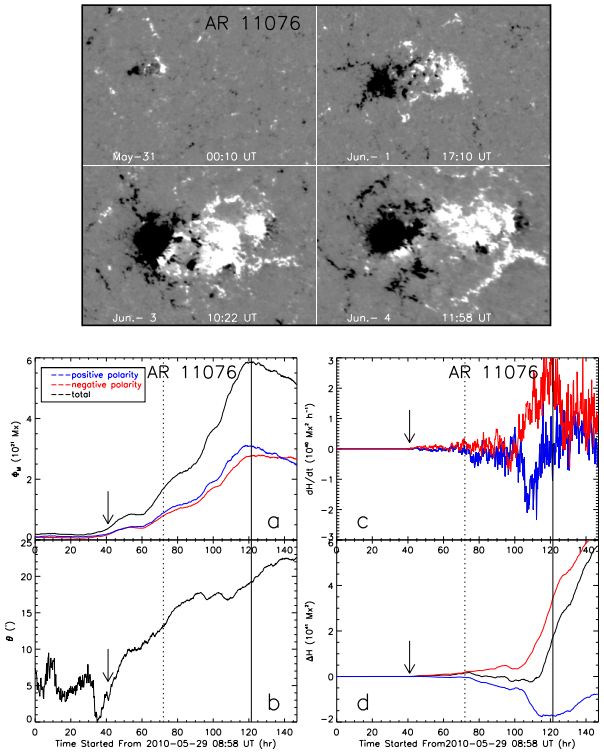

Figure 2. Same as Figure 1, but for AR 11076

3. RESULTS

3.1. AR 11072 and AR 11076

AR 11072 first emerged at southern hemisphere (S15E36) on May 20, 2010 and passed the solar disc center three days later, while AR 11076 emerged at southern hemisphere (S19E19) on May 31, 2010 and passed through the disc center on June 1. The emergence process of AR 11072 lasted for about 40 hr, and then it developed into a bipolar structure with a compact leading polarity and a fragmented following polarity. AR 11076 also possessed a bipolar structure during its life time passing the solar disc. Unlike normal bipolar ARs, AR11076 showed a compact following polarity and a dispersed leading polarity. The morphological evolution of the two ARs, AR11072 and AR11076, are briefly discussed in the upper panels of Figures 1 and 2 in four snapshots of SDO/HMI line of sight magnetograms. The leading polarity of AR 11072, with positive magnetic field, is clearly more compact and barely decayed during the observation. The following polarity, with negative magnetic field, however, is quite fragmented and decayed very quick. As for AR 11076, it had the same sign of magnetic field for each polarity as AR 11072, but both polarities were compact to begin with, and then the leading polarity slowly decayed and became fragmented.

The evolution of magnetic flux and polarity distance of the two ARs are measured by means of HMI magnetograms. The results are plotted in bottom panels

Table 1
Nine emerging bipolar ARs[a]

NOAA	CMD	Pos	Pol	$\Delta\Phi_L/\Delta\Phi_F$	$\Delta H_L/\Delta H_F$	$(\Delta H_L)_f/(\Delta H_F)_f$	$(\Delta H_L)_s/(\Delta H_F)_s$
11072	May 23	S15E36	Positive	16.6/-15.1	-106.9/3.2	-77.6/1.6	-29.3/1.6
11076	Jun 1	S19E19	Positive	23.4/-25.8	-7.9/65.3	-17.3/34.5	9.4/30.8
11120	Nov 6	N13E13	Negative	-6.6/6.4	1.1/3.8	1.4/1.9	-0.3/-2.0
11124	Nov 13	N14E42	Negative	-41.9/34.1	-88.1/59.3	-125.0/35.5	36.9/23.8
11130	Nov 29	N13E23	Negative	-35.2/31.6	-60.6/-118.2	15.6/-91.8	-76.2/-26.5
HARP							
0044	Jun 2	S33E20	Positive	1.0/-1.3	-1.9/1.4	-1.1/1.2	-0.8/0.2
0047	Jun 9	N15E32	Negative	-1.8/0.9	-0.5/-1.0	0.3/0.4	-0.8/-1.4
0228	Oct 18	N18E00	Negative	-1.0/0.4	0.077/0.211	-0.074/0.067	0.151/0.144
0296	Dec 10	S16E14	Positive	1.0/-2.0	-0.7/-2.7	0.3/-0.9	-1.0/-1.8

Notes. [a] Pos denotes the latitude and longitude at which the AR started emerging, and Pol denotes the sign of the magnetic field in the leading polarity. $\Delta\Phi_L$ and $\Delta\Phi_F$ denote the magnetic flux of leading and following polarities, respectively (in units of $10^{20}Mx$), and ΔH_L and ΔH_F denote the magnetic helicity flux injected by leading and following polarities, respectively (in units of $10^{40}Mx^2$), and $(\Delta H_L)_f/(\Delta H_F)_f$ and $(\Delta H_L)_s/(\Delta H_F)_s$ denote the helicity of leading and following polarities before and after the reference time, respectively (in units of $10^{40}Mx^2$).

of Figure 1 and Figure 2. Panel a in Figure 1 represents the 6-day changes of magnetic flux in AR 11072, with blue, red, and black curves that denote temporal profiles of positive, negative, and unsigned magnetic fluxes, respectively. Panel b in Figure 1 represents the polarity distance of AR 11072, which is the distance between the barycentre of its two polarities. The arrows mark the first emergence of AR 11072, while the vertical solid lines indicate the time when the unsigned magnetic flux reached its maximum, and the vertical dotted lines mark the time when the active regions pass through the central meridian of the observed solar disk. We find that the magnetic flux of AR 11072 started rising close to 25 hr and lasted for till about 40 hr. The unsigned flux increase from around 0 to 5×10^{21} Mx, while the polarity distance grew from zero to $18''$. Then the magnetic flux ceased increasing, for about 10 hr, and fell slowly and eventually dropped to 3.5×10^{21} Mx. It is also clear that the changes of the polarity distance behaves quite like the magnetic flux: it first increases, then ceases, and finally drops slowly. It is noted that through the entire 6-day observation, the magnetic flux of leading and following polarity are approximately equivalent to each other, with the leading polarity slightly higher than the following one. The change of magnetic flux (panel a) and polarity distance (panel b) of AR 11076 is shown in the Figure 2. The image panels of Figure 2 are arranged similar to Figure 1. The unsigned magnetic flux of AR 11076 evolves quite similar to AR 11072: i.e., it began to increase after its first emergence, then reached its maximum, 5.8×10^{21} Mx 80 hr later, and finally began to fall. The negative magnetic flux (the following polarity), however, did not decrease but stayed steady while the unsigned flux began falling. Unlike AR 11072, the polarity distance in AR 11076 was increasing all the time except from 90 to 110 hr. Such behavior indicates a different evolution process in AR 11076. In this case, the two polarities keep separating from each other throughout the observation, while the polarities in AR 11072 separate from each other in the beginning, and then stop separating since its unsigned magnetic flux began to decrease. Similar to AR11072, the magnetic flux of the leading and the following polarities of AR11076 are approximately equal to each other. However, on an average, the leading polarity flux tends to be slightly higher than that of the following polarity.

The injection rate of magnetic helicity and accumulated magnetic helicity flux of AR 11072 and 11076 were measured too. We derived the photospheric flow velocity by applying the DAVE method to the HMI data and calculated the magnetic helicity density according to G_θ. Both AR 11072 and 11076 processed well-formed bipolar structures and their tilt angles to the equator were very small, which can be seen from their morphological evolution. We used the area integral of the magnetic helicity density over leading/following polarity as the injection rate of magnetic helicity of each polarity. The results are plotted in panels c and d in Figure 1 and Figure 2. The blue/red curves represent fluxes from the positive/negative polarities, and black curve represents the total flux. It is obvious that the leading polarity of AR 11072 prevails in the injection rate of the magnetic helicity. Temporal variations of the magnetic helicity flux between the following and leading polarities are also different from each other. The leading polarity injects about 33 times more magnetic helicity flux than the following one. These results agree with the former study conducted by Tian & Alexander (2009) and Fan et al. (2009). According to their explanation, the discrepancy of the magnetic helicity between the polarities is caused by the significantly faster emergence of the leading polarity. As for AR 11076, however, it is the following polarity that injected more helicity, about 8 times more than the leading polarity. The result seems to contradict previous studies. However, the polarity morphology of the bipolar emerging ARs studied previously, which consist of a compact leading polarity and a fragmented following one, is different from AR 11076. This difference can be a possible reason for the contra-

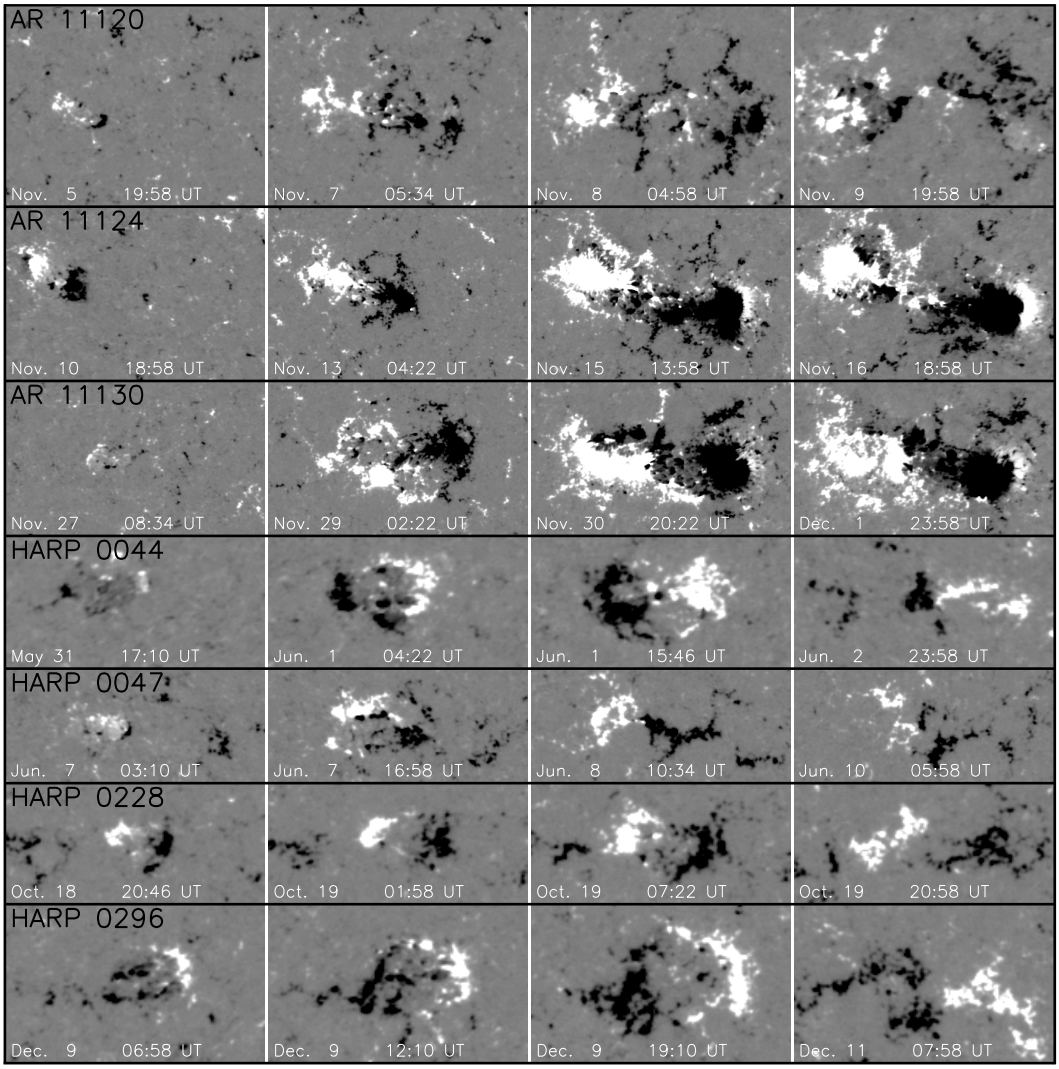

Figure 3. HMI 12-min line-of-sight magnetograms of AR 11120, 11124, and 11130, and HARP 0044, 0047, 0228, and 0296, showing their emergence processes.

dictory results.

To see how the discrepancy varies with time, we divide the emergence process into two evolutionary stages based on the change of the unsigned magnetic flux. The two stages are separated by the time when the unsigned magnetic flux reached its maximum, which is the vertical solid line Figure 1 and Figure 2. We can see obvious difference in the injection rate of the magnetic helicity between the two stages. In AR 11072, the injection rate of both polarities became smaller after the reference time, while the leading polarity even changed its sign around the the vertical solid line. For AR 11076 the injection rate of the following polarity did not change much, and the leading polarity changed significantly from negative to positive after the reference time. The ratio of the accumulated magnetic helicity flux between the leading and following polarities also changed between the two stages. It varied from 48 to 18 in AR 11072, and -0.5 to 0.3 in AR 11076. These results imply a time dependance of the asymmetry of the magnetic helicity. For other detailed information about AR 11072, one may refer to the results of Liu & Schuck (2012).

3.2. The Other Seven ARs

The morphological evolution of the other seven ARs, AR 11120, 11124, and 11130, and HARP 0044, 0047, 0228, and 0296, are shown in Figure 3, with four snapshots of HMI line-of-sight magnetogram for each AR. Their emerging information is listed in Table 1. All seven ARs we selected possess well-formed bipolar structures and satisfy Joy's law. AR 11130 has a compact leading polarity and a low fragmented following polarity, while AR 11120 has a fragmented leading polarity and a compact following polarity. The rest of the ARs do not show any clear sign of relative compactness of polarities. The diversity of the polarity morphology in our case may show a different result on the helicity asymmetry from previous works. We measured the magnetic flux and calculated the injected

magnetic helicity of all ARs, using the same method as mentioned above, and plotted their 6-day evolution of magnetic flux (panel a), magnetic helicity injection rate (panel b), and accumulated magnetic helicity flux (panel c) in Figures 4 and 5. The figures demonstrate that the ARs without NOAA numbers show typically an order of magnitude lower magnetic flux than those with NOAA numbers. Additionally, they take lesser time to evolve from emergence to decay as compared to the ARs with NOAA numbers. The difference of magnetic flux between leading and following polarities in all ARs is very small. The accumulated magnetic helicity injected through the two polarity, however, is quite different, i.e., they all have a prevailing polarity in injecting magnetic helicity flux. While most ARs show higher magnetic helicity flux in their following polarities, AR 11124 and HARP 0044 show significantly higher flux in their leading polarities.

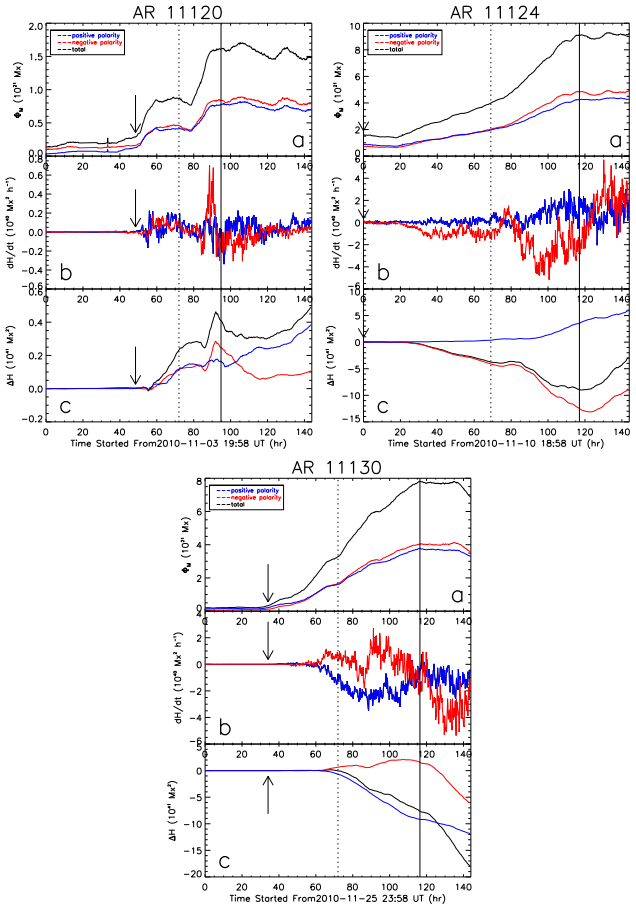

Figure 4. Changes of the magnetic flux (a), magnetic helicity flux (b), and the accumulated magnetic helicity flux (c) for AR 11120, 11124, and 11130. The blue/red curves denote the flux of positive/negative polarity. The arrows mark the first emergence, and the vertical solid lines indicate the time when the unsigned magnetic flux reached its maximum, and the vertical dotted lines mark the time when the active regions pass through the central meridian on the observed solar disk.

We also divided the emergence of the ARs into two stages, using the same method as that adopted for AR 11072 and 11076. The results are listed in Table 1. $\Delta\Phi_L$ and $\Delta\Phi_F$ denote the magnetic flux of leading and following polarities, respectively, and ΔH_L and ΔH_F represent the magnetic helicity flux injected by leading and following polarities, and $(\Delta H_L)_f/(\Delta H_F)_f$ and $(\Delta H_L)_s/(\Delta H_F)_s$ denote the helicity of leading and following polarities of two stages, respectively. Significant difference in the accumulated magnetic helicity flux can be found in the two evolutionary stages of these ARs. AR 11124 and 11130 and HARP 0228 and 0296 have one polarity that changed the sign of magnetic helicity flux during transition from the first stage to the second stage, while AR 11120 and HARP 0047 have both polarities that changed the helicity sign. The prevailing polarity in the injection of magnetic helicity flux of AR 11130 and HARP 0044 changed from the following polarity to the leading polarity. Most interesting result occurred in HARP 0228. The leading polarity of this AR injected more magnetic helicity flux in both stages, while its following polarity injected more magnetic helicity flux in the whole period of flux emergence.

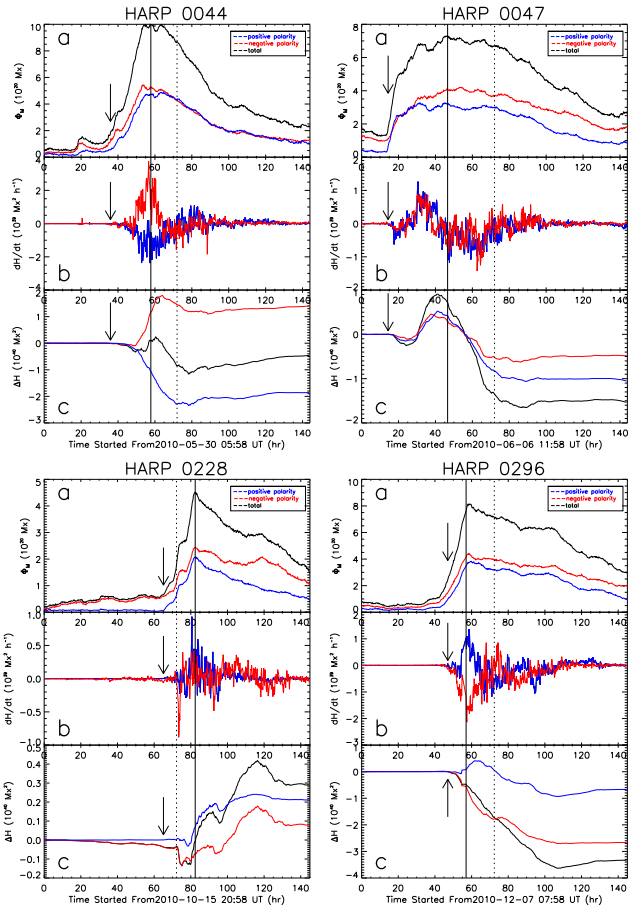

Figure 5. Same as Figure 4, but for HARP 0044, 0047, 0228, and 0296.

Table 2
Nine emerging bipolar ARs[a]

NOAA	$\overline{S}_L/\overline{S}_F$	$(\overline{S}_L)_f/(\overline{S}_F)_f$	$(\overline{S}_L)_s/(\overline{S}_F)_s$	$\overline{B}_L/\overline{B}_F$	$(\overline{B}_L)_f/(\overline{B}_F)_f$	$(\overline{B}_L)_s/(\overline{B}_F)_s$
11072	8.3/10.9	6.2/7.9	11.2/14.9	206/-150	216/-171	199/-135
11076	8.6/6.8	6.8/5.3	17.5/14.3	145/-167	137/-154	160/-191
11120	5.6/3.9	4.2/3.0	9.1/6.0	-90/115	-90/110	-90/122
11124	14.8/14.0	12.4/12.4	25.4/22.4	-176/169	-170/159	-188/192
11130	9.2/10.8	7.3/8.6	17.2/20.1	-209/170	-196/163	-231/181
HARP						
0044	2.2/2.6	1.3/2.1	2.7/2.9	92/-85	92/-78	92/-88
0047	3.3/2.3	2.9/2.1	3.6/2.4	-84/86	-87/95	-84/82
0228	1.4/0.7	1.0/0.3	2.0/1.2	-79/88	-61/77	-91/92
0296	1.9/2.6	0.9/1.5	2.5/3.4	93/-87	69/-64	98/-94

Notes. [a] $\overline{S}_L/\overline{S}_F$ denotes the mean area of leading/following polarity (in units of $10^{18}cm^2$), and $(\overline{S}_L)_f/(\overline{S}_F)_f$ and $(\overline{S}_L)_s/(\overline{S}_F)_s$ represent the mean aera of leading/following polarity before and after the reference time (in units of $10^{18}cm^2$), and $\overline{B}_L/\overline{B}_F$ denote the mean magnetic field of leading/following polarity (in units of G), and $(\overline{B}_L)_f/(\overline{B}_F)_f$ and $(\overline{B}_L)_s/(\overline{B}_F)_s$ represent the mean magnetic field strength of leading/following polarity before and after the reference time (in units of G).

4. Discussion and Summary

We applied DAVE to SDO/HMI 12-min line-of-sight magnetograms with 9 emerging bipolar ARs. We studied not only ARs having a compact leading polarity and a fragmented following polarity as well as other kinds of polarity morphology of emerging bipolar ARs. Five of the ARs included in our study are AR 11072, 11075, 11120, 11124, and 11130. The other four ARs are too small to have a NOAA number and are identified by the HARP program. These are HARP 0044, 0047, 0228 and 0296. We measured the magnetic flux, calculated the injection rate of magnetic helicity for the leading and the following polarities of the ARs, and divided the emergence process into two evolutionary stages, by using the time when their unsigned magnetic flux reached maximum as reference. We then calculated the magnetic helicity flux of the two stages. The main results of our work are summarised as follows. (1) All ARs have a prevailing polarity in injecting magnetic helicity flux, while the magnetic flux of their two polarities is approximately equal to each other. Six ARs we studied (AR 11075, 11124, and 11130 and HARP 0047, 0228 and 0296) have the following polarity that injected more magnetic helicity flux than that of the leading one. (2) Clear changes in the asymmetry of the magnetic helicity flux was found in their two evolutionary stages. Seven ARs had one or both polarities that changed sign of magnetic helicity flux during transition from one stage to another. The prevailing polarity of magnetic helicity flux in AR 11130 and HARP 0044 changed form the following polarity to the leading one.

The asymmetry of the magnetic helicity flux in our case seems quite different from previous results. However, it should be noted that the bipolar active regions in the previous studies were selected by the condition that their leading polarity is more compact than their following polarity. In our case, only two ARs, AR 11072 and 11130, evidently satisfy such polarity morphology, while AR 11076 and 11120 have the opposite polarity morphology. It is difficult to comment on the relative compactness of polarities of the other five ARs. To compare our results with previous results, we need to estimate the relative compactness of polarities. Therefore, we measured mean area and the mean magnetic field strength of each polarity in all 9 ARs, considering the region where magnetic flux is greater than 20 G (less than -20 G) as the positive (negative) polarity. The results are listed in the Table 2. We can see that four ARs contain a leading polarity with a smaller mean area (AR 11072 and 11130 and HARP 0044 and 0296), while the leading polarities of five ARs contain a larger mean area (AR 11076, 11120, 11124 and HARP 0047 and 0228). We find that ARs of with leading polarities showing higher average magnetic field strength, usually have a more compact leading polarity and vice versa. Additionally 7 out of 9 ARs, except AR 11130 and HARP 0296, have a compact polarity that prevail in the injection of magnetic helicity flux, implying a correlation between polarity compactness and magnetic helicity injection. Tian & Alexander (2009) and Fan et al. (2009) have pointed out that polarities with higher magnetic field strength could be more buoyant and emerge faster. The polarity morphology of the ARs used in Tian & Alexander (2009) and Tian et al. (2011) is only a compact leading polarity and a fragmented following one. This leads to the leading polarity injecting more helicity than the following polarity. However, we also include the opposite polarity morphology in this study. Considering the morphology of polarities, our results agree with the previous works, and also suggest that the compact polarity tends to have more magnetic helicity flux than the fragmented one. It should be noted that observations indicate that bipolar ARs tend to possess a compact leading polarity and a fragmented following polarity. Theoretical studies suggest such polarity morphology could be formed by coriolis force acting on the emerging flux tubes, which could bend the rising tubes and produce a greater magnetic field in the leading side (Fan et al. 1993; Fisher et al. 2000; Fan et al. 2009). A recent study on the area asym-

metry of bipolar ARs, which uses MDI magnetograms from April 23, 1996 to September 2, 2001, show that 37% (51 out of 138) ARs have a larger leading polarity than the following ones (Yamamoto 2012). Such results confirm our perception of the area asymmetry in bipolar ARs. However, according to this study, a certain number of ARs (about 37%), should possess a more compact following polarity, meaning a common presence of a more compact following polarity morphology in bipolar ARs. We thus suggest more ARs should have a following polarity that emerge faster and inject more magnetic helicity.

Seven ARs we studied have shown a reversed sign of the magnetic helicity flux in at least one polarity. Many other studies have also reported reversal in the sign of magnetic helicity flux (Zhang et al. 2008; Park et al. 2010; Ravindra et al. 2011; Park et al. 2012). We try to attribute the sign reversal of the magnetic helicity flux to the change of relative strength of the mean magnetic field strength. However, only three ARs (AR 11124 and HARP 0047 and 0296) have some change in the relative mean field strength, while the prevailing polarity of these ARs in the injection of magnetic helicity flux did not change in the two stages. This suggests that the relative strength of mean magnetic field strength may not responsible for the changes. Since most of ARs we studied showed a reversed sign in injecting magnetic helicity flux, such sign reversal might be a common phenomenon in emerging bipolar ARs. However, the reason of such a behaviour is still unexplained. Also, we cannot explain why AR 11130 and HARP 0296 have a less compact polarity that prevail in the injection of magnetic helicity flux. We understand that the emergence of the magnetic flux tubes accompanied by magnetic helicity injection is a very complicated process. More efforts are needed before we fully understand its physics.

Acknowledgments

We thank an anonymous referee for providing detailed suggestions and comments that significantly improved the presentation of this paper. We thank the HMI teams and HARPs program for data support. This work is supported by the 973 Program (2011CB811403), by the Natural Science Foundation of China under grants 11173058, 11273056, and 11333007 and by the CAS grant KJCX2-EW-T07.

References

Berger, M. A. 1984, Rigorous New Limits on Magnetic Helicity Dissipation in the Solar Corona, GApFD, 30, 79

Berger, M. A., & Field, G. B. 1984, The Topological Properties of Magnetic Helicity, JFM, 147, 133

Chae, J. 2001, Observational Determination of the Rate of Magnetic Helicity Transport through the Solar Surface via the Horizontal Motion of Field Line Footpoints, ApJ, 560, L95

Chae, J. 2007, Measurements of Magnetic Helicity Injected through the Solar Photosphere, AdSpR, 39, 1700

Démoulin, P., Mandrini, C. H., Van Driel-Gesztelyi, L., Lopez Fuentes, M. C., & Aulanier, G. 2002, The Magnetic Helicity Injected by Shearing Motions, Sol. Phys., 207, 87

Démoulin, P., & Pariat, E. 2009, Modelling and Observations of Photospheric Magnetic Helicity, AdSpR, 43, 1013

Fan, Y., Alexander, D., & Tian, L. 2009, On the Origin of the Asymmetric Helicity Injection in Emerging Active Regions, ApJ, 707, 604

Fan, Y., Fisher, G. H., & Deluca, E. E. 1993, Solar Activity, Solar Magnetic Field, Solar Physics, Coriolis Effect, Mathematical Models, Solar Interior, Sunspots, ApJ, 405, 390

Fisher, G. H., Fan, Y., Longcope, D. W., Linton, M. G., & Pevtsov, A. A. 2000, The Solar Dynamo and Emerging Flux - (Invited Review), Sol. Phys., 192, 119

Hao, J., & Zhang, M. 2011, Hemispheric Helicity Trend for Solar Cycle 24, ApJ, 733, L27

Leka, K. D., Canfield, R. C., McClymont, A. N., & van Driel-Gesztelyi, L. 1996, Evidence for Current-Carrying Emerging Flux, ApJ, 462, 547

Leka, K. D., Fan, Y., & Barnes, G. 2005, On the Availability of Sufficient Twist in Solar Active Regions to Trigger the Kink Instability, ApJ, 626, 1091

Liu, J., & Zhang, H. 2006, The Magnetic Field, Horizontal Motion and Helicity in a Fast Emerging Flux Region which Eventually Forms a Delta Spot, Sol. Phys., 234, 21

Liu, Y., & Schuck, P. W. 2012, Magnetic Energy and Helicity in Two Emerging Active Regions in the Sun, ApJ, 761, 105

Longcope, D. W., Fisher, G. H., & Pevtsov, A. A. 1998, Flux-Tube Twist Resulting from Helical Turbulence: The Sigma-Effect, ApJ, 507, 417

Longcope, D. W., & Pevtsov, A. A. 2003, Helicity Transport and Generation in the Solar Convection Zone, AdSpR, 32, 1845

Low, B. C. 1996, Solar Activity and the Corona, Sol. Phys., 167, 217

Pariat, E., Démoulin, P., & Berger, M. A. 2005, Photospheric Flux Density of Magnetic Helicity, A&A, 439, 1191

Pariat, E., Nindos, A., Démoulin, P., & Berger, M. A. 2006, What is the Spatial Distribution of Magnetic Helicity Injected in a Solar Active Region?, A&A, 452, 623

Park, S. H., Chae, J., Jing, J., Tan, C., & Wang, H. 2010, Time Evolution of Coronal Magnetic Helicity in the Flaring Active Region NOAA 10930, ApJ, 720, 1102

Park, S. H., Cho, K. S., Bong, S. C., et al. 2012, The Occurrence and Speed of CMEs Related to Two Characteristic Evolution Patterns of Helicity Injection in Their Solar Source Regions, ApJ, 750, 48

Pevtsov, A. A. 2008, What Helicity Can Tell Us about Solar Magnetic Fields, JApA, 29, 49

Pevtsov, A. A., & Balasubramaniam, K. S. 2003, Helicity Patterns on the Sun, AdSpR, 32, 1867

Pevtsov, A. A., Canfield, R. C., & Metcalf, T. R. 1995, Latitudinal Variation of Helicity of Photospheric Magnetic Fields, ApJ, 440, L109

Pipin, V. V., Zhang, H., Sokoloff, D. D., Kuzanyan, K. M., & Gao, Y. 2013, The Origin of the Helicity Hemispheric Sign Rule Reversals in the Mean-field Solar-type Dynamo, MNRAS, 435, 2581

Ravindra, B., Yoshimura, K., & Dasso, S. 2011, Evolution of Spinning and Braiding Helicity Fluxes in Solar Active Region NOAA 10930, ApJ, 743, 33

Rust, D. M. 1994, Spawning and Shedding Helical Magnetic

Fields in the Solar Atmosphere, GeoRL, 21, 241
Schou, J., Antia, H. M., Basu, S., et al. 1998, Helioseismic Studies of Differential Rotation in the Solar Envelope by the Solar Oscillations Investigation Using the Michelson Doppler Imager, ApJ, 505, 390
Schuck, P. W. 2005, Local Correlation Tracking and the Magnetic Induction Equation, ApJ, 632, L53
Schuck, P. W. 2006, Tracking Magnetic Footpoints with the Magnetic Induction Equation, ApJ, 646, 1358
Schuck, P. W. 2008, Tracking Vector Magnetograms with the Magnetic Induction Equation, ApJ, 683, 1134
Seehafer, N. 1996, Nature of the α Effect in Magnetohydrodynamics, Phys. Rev. E, 53, 1283
Taylor, J. B. 1974, Relaxation of Toroidal Plasma and Generation of Reverse Magnetic Fields, PhRvL, 33, 1139
Taylor, J. B. 1986, Relaxation and Magnetic Reconnection in Plasmas, RvMP, 58, 741
Tian, L., & Alexander, D. 2009, Asymmetry of Helicity Injection Flux in Emerging Active Regions, ApJ, 695, 1012
Tian, L., Démoulin, P., Alexander, D., & Zhu, C. 2011, On Asymmetry of Magnetic Helicity in Emerging Active Regions: High-Resolution Observations, ApJ, 727, 28
Wachter, R., Schou, J., Rabello-Soares, M. C., et al. 2012, Image Quality of the Helioseismic and Magnetic Imager (HMI) Onboard the Solar Dynamics Observatory (SDO), Sol. Phys., 275, 261
Wang, C., & Zhang, M. 2010, A Hemispheric Helicity Sign Rule Indicated by Large-Scale Photospheric Magnetic Fields at Three Phases of Solar Cycle 23, ApJ, 720, 632
Wang, J. 1996, A Note on the Evolution of Magnetic Helicity in Active Regions, Sol. Phys., 163, 319
Wang, J., Zhou, G., & Zhang, J. 2004, Helicity Patterns of Coronal Mass Ejection-Associated Active Regions, ApJ, 615, 1021
Wang, Y. M. 2013, On the Strength of the Hemispheric Rule and the Origin of Active-region Helicity, ApJ, 775, L46
Welsch, B. T., Abbett, W. P., De Rosa, M. L., et al. 2007, Tests and Comparisons of Velocity-Inversion Techniques, ApJ, 670, 1434
Woltjer, L. 1958, A Theorem on Force-Free Magnetic Fields, PNAS, 44, 489
Yamamoto, T. T. 2012, The Area Asymmetry in Bipolar Magnetic Fields, A&A, 539, A13
Yeates, A. R., & Mackay, D. H. 2009, Modelling the Global Solar Corona: III. Origin of the Hemispheric Pattern of Filaments, Sol. Phys., 254, 77
Zhang, H., Sakurai, T., Pevtsov, A., et al. 2010, A New Dynamo Pattern Revealed by Solar Helical Magnetic Fields, MNRAS, 402, L30
Zhang, M., Flyer, N., & Low, B. C. 2006, Magnetic Field Confinement in the Corona: The Role of Magnetic Helicity Accumulation, ApJ, 644, 575
Zhang, Y., Tan, B., & Yan, Y. 2008, Correlation between the Sharp Variation of the Transport Rate of Magnetic Helicity and Solar Eruptive Events, ApJ, 682, L133
Zhao, J., & Kosovichev, A. G. 2004, Torsional Oscillation, Meridional Flows, and Vorticity Inferred in the Upper Convection Zone of the Sun by Time-Distance Helioseismology, ApJ, 603, 776